

Damage of concrete in a very high stress state: experimental investigation

C. Poinard · Y. Malecot · L. Daudeville

Received: 3 July 2008 / Accepted: 23 December 2008 / Published online: 9 January 2009
© RILEM 2009

Abstract This study is intended to characterize the evolution in triaxial behavior of a standard concrete subjected to confining pressures varying from 0 to 600 MPa. Hydrostatic and triaxial tests, with several unloading–reloading cycles, are carried out on concrete samples using a high-capacity triaxial press. These tests serve to identify the evolution of the elastic unloading characteristics of concrete, depending on both confining pressure and axial strain. A number of optical observations are also provided to allow visualizing the evolution in concrete damage mode in the middle of the sample. Experimental results indicate a sizable change in concrete behavior with confining pressure. At low pressure values, Young’s modulus decreases and Poisson’s ratio rises sharply with axial strain. The concrete exhibits brittle behavior with failure caused by a localized damage mechanism. In contrast, at high confining pressures, the concrete becomes a ductile material, and the evolution in its unloading characteristics is negligible. Failure is thus associated with diffuse material

damage. The concrete behaves like a granular material controlled by plasticity, meaning that the damage phenomenon observed at low confinement is completely inhibited.

Keywords Concrete · Triaxial test · High confining pressure · Unloading–reloading cycles · Young’s modulus · Poisson’s ratio

1 Introduction

This article focuses on the behavior of concrete under extreme loading conditions (e.g. near-field detonations, ballistic impacts). During such loadings, concrete is subjected to very high-intensity stress states. As an illustration, when a rigid projectile impacts a massive concrete structure, three triaxial behavior phases can be observed, each one corresponding to different damage modes that may in some cases occur simultaneously [1]. The validation of concrete behavior models, which simultaneously incorporate the phenomena of brittle damage and irreversible strain such as compaction, thus requires test results that enable reproducing the kind of complex loading paths described previously.

Most experimental results available in the literature only address triaxial loadings with a moderate level of confining pressure [2–8]. In particular, these authors have revealed the transition from brittle to

C. Poinard (✉) · Y. Malecot · L. Daudeville
Laboratoire Sols Solides Structures – Risques,
Université Joseph Fourier – Grenoble I,
38041 Grenoble cedex 9, France
e-mail: cedric.poinard@hmg.inpg.fr

Y. Malecot
e-mail: yann.malecot@ujf-grenoble.fr

L. Daudeville
e-mail: laurent.daudeville@ujf-grenoble.fr

ductile behavior in characterizing cohesive materials. The results presented in this article refer to triaxial compression tests conducted on concrete samples by means of a high-capacity hydraulic triaxial press, called GIGA. This experimental device makes it possible to generate stress levels within the samples on the order of 1 GPa with static, homogeneous and well-controlled loading paths.

Deriving the static characterization of a constitutive model for the purpose of predicting dynamic calculations is not a new practice within the study of geomaterials. Previous experimental studies have essentially been limited to mortar samples [9–11]; such studies emphasize both the increase in mortar deviatoric stress and the evolution in mortar limit states with confinement. The aim of the present paper is to extend this practice to the study of an “actual” concrete material (i.e. with an aggregate dimension on the order of a centimeter). The comparative evaluation between a concrete and a mortar with confining pressure reaching 500 MPa, as conducted by Akers [12], highlights the differences in behavior between two materials and moreover reveals that the study of mortar with strong confinement is not representative of concrete behavior. Other triaxial test results on ordinary concrete with confining pressures ranging between 0 and 500 MPa yield the evolution in concrete behavior and limit states with confinement [13, 14].

In 2004, the university of Grenoble launched, in collaboration with the Centre d’Etude de Gramat (DGA, French Defense Ministry), a research program on the vulnerability of concrete infrastructure. During a previous stage of this program that utilized the same baseline material, Gabet assessed the influence of loading paths on concrete behavior [15]. Among other things, these results indicated that under high confinement, the limit state of concrete remains relatively independent of both the loading path and Lode’s angle. Keep in mind however that this experimental study only examined the monotone triaxial test (i.e. in the absence of loading–unloading cycles). The task of identifying, through these tests, behavior models that actually couple damage and plasticity remains quite difficult.

By performing cyclic tests using several loading–unloading–reloading cycles, this article seeks to describe the overall behavior of concrete in greater detail. The reversible part of strain along with the

eventual relevant damage will be dissociated from the irreversible strain related to material plasticity. Moreover, concrete behavior will be correlated with damage mode by performing an optical analysis on the test samples.

Only a few studies in the literature describe the evolution in elastic concrete parameters during triaxial testing at high confinement. For a triaxial compression test at 40 MPa of confinement, Sfer produced results showing a very slight decrease in the Young’s modulus of concrete with axial strain [8]. Lu presented similar tests on high-strength concrete. These results indicate that the Young’s modulus of concrete only decreases very minimally and that hysteresis phenomena appear with an increase in axial strain [16]. This set of results differs in comparison with a simple compression test, which yields a strong increase in Poisson’s ratio and a sizable drop in Young’s modulus [17].

Many authors have concentrated on the mode of failure found in cement matrix materials for triaxial compression tests up to 60 MPa of confinement. For very low levels of confining pressure, failure is caused by crack propagation parallel to the primary load direction. As confinement rises, these cracks become less frequent and oriented in a sidewise direction within this frame of reference [8, 18]. Yet the literature does not contain any description of concrete failure modes for higher confinements.

The study presented herein is therefore aimed at completing these previous research efforts by focusing on the concrete failure mechanism for triaxial compression tests ranging from simple compression to 600 MPa of confinement. The experimental devices used for both this testing and the optical analysis of samples will be described in Sect. 2. Test results and corresponding optical observations will be presented next (Sect. 3). The effects of an increase in confinement on concrete behavior, in particular on damage evolution, will then be deduced and set forth in Sect. 4.

The article will close in Sect. 5 with a discussion of the primary results from this experimental study.

2 Experimental instrumentation

2.1 Triaxial cell

The tests have been conducted with a high-capacity triaxial press that allows loading a cylindrical



concrete specimen 7 cm in diameter and 14 cm long. Figure 1 shows a general view of the press. A cross-section of the confining cell is provided in Fig. 2. This press is able to generate a confining pressure of up to 0.85 GPa and an axial stress reaching 2.3 GPa. The concrete specimen is placed in the confining cell, and the confining fluid, diethylhexyl azelate—a non-volatile organic liquid, is injected into the cell through the upper opening. The cell is then pressurized by means of a multiplying jack. The axial force

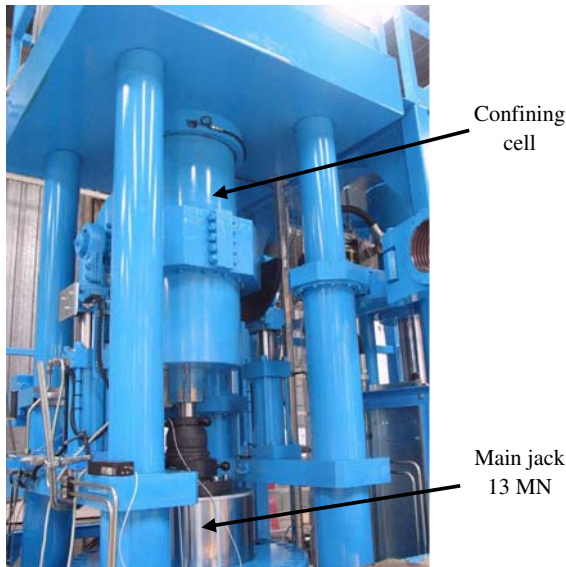


Fig. 1 General view of the GIGA press

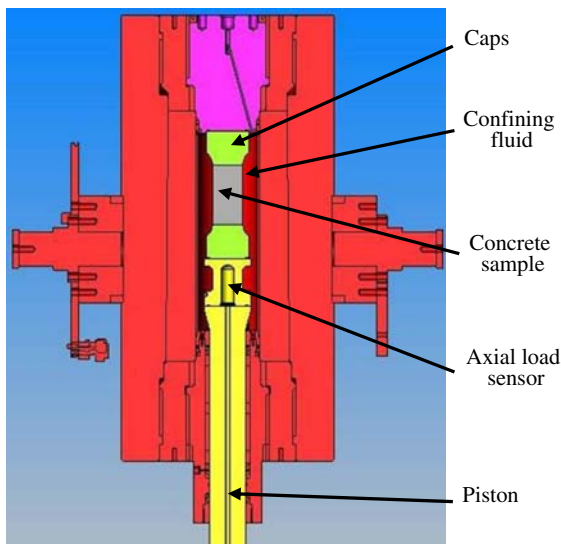


Fig. 2 Cross-section of the confining cell

is generated from a 13-MN jack placed underneath the cell; this force is transmitted to the specimen via a piston that passes through the lower cell plug. An axial displacement sensor located on the machine is used to control axial jack displacement, while an axial load sensor and pressure sensor positioned inside the confining cell yield the stress state on the specimen. Both the confining pressure and jack axial displacement are servo-controlled, which offers several potential loading paths.

2.2 Preparation of the concrete sample

The concrete composition, which is identical to that used by Gabet and Vu, is provided in Table 1. This mix proportioning corresponds to an ordinary concrete in terms of both strength and slump.

After pouring, the concrete blocks were conserved for 1 month in water and then machined and stoked for 2 months in a drying oven at 50°C, which made the concrete practically dry at the time of testing (i.e. with a saturation level of concrete equal to approximately 11%).

The level of strain is measured by means of an axial LVDT sensor, an axial gauge and two circumferential gauges. Strain measurement redundancy serves to increase the probability of maintaining the same measurement until the end of the test as well as to check sample strain homogeneity. It will be shown in Sect. 4 that the latter is well satisfied during the triaxial tests. The effect of friction at the specimen ends is then negligible during triaxial tests under high

Table 1 Compositions and mechanical properties of the studied concrete

<i>Concrete composition</i>	
0.5/8 “D” gravel (kg/m ³)	1,008
1,800 μm “D” sand (kg/m ³)	838
CEM I 52.5 N PM ES CP2 cement (Vicat) (kg/m ³)	263
Water (kg/m ³)	169
Density (kg/m ³)	2,278
<i>Mechanical properties of the concretes</i>	
Average tested strength after 28 days (MPa)	29
Average slump measured using the Abrams cone (cm)	7
Volume of occluded air measured in fresh concrete (%)	3.4
Porosity accessible to water (%)	12
W/C ratio	0.64
Cement paste volume V_p (m ³ /m ³)	0.252

confinement and nothing has been done to reduce it. Only for the simple compression tests a special lubricant has been used.

Considering the porous nature of concrete, this high level of confining pressure has necessitated developing a protective multilayer membrane around the sample, composed of 8 mm of latex and 2 mm of neoprene [19, 20].

2.3 Loading path

In this article, stresses are considered positive in compression. σ_x denotes axial stress, p the confining pressure (Fig. 3), σ_m the mean stress and q the scalar deviatoric stress, such that:

$$\sigma_m = \frac{\sigma_x + 2p}{3} \quad (1)$$

$$q = \sigma_x - p \quad (2)$$

Two different kinds of tests are performed as part of this study. The first consists of a hydrostatic load with several unloading–reloading cycles of increasing intensity. The cycles are composed of the following confining pressures in succession: $p = 10, 20, 30, 40, 50, 80, 100, 150, 200, 300, 400$ and 580 MPa (Fig. 4). For the first four cycles, the pressure variation rate equals 0.5 MPa/s; for the subsequent cycles, this rate climbs to 1.67 MPa/s.

Except for the simple compression test, all tests have been conducted using a triaxial loading path. The test begins by applying a hydrostatic load, during which confining pressure increases at a rate of

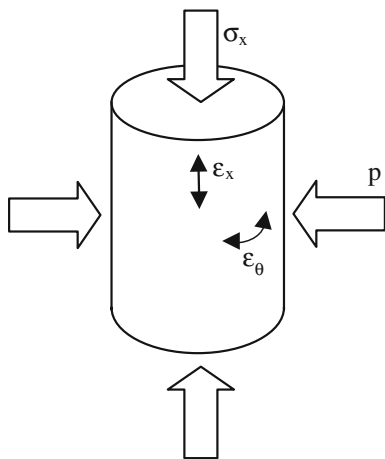


Fig. 3 Diagram depicting sample stresses and strains

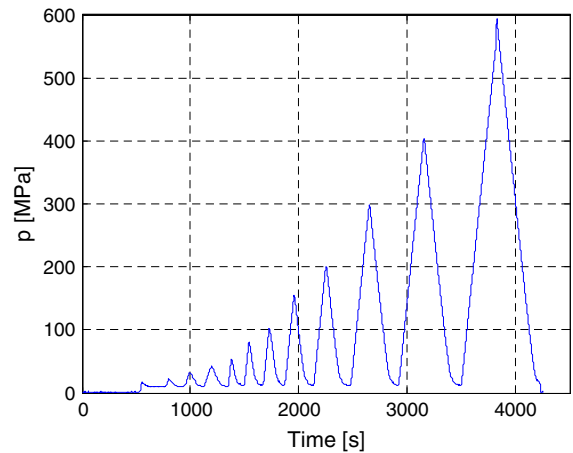


Fig. 4 Hydrostatic test (HYD): confining pressure versus time

1.67 MPa/s until reaching the desired pressure. While holding confining pressure stable, the sample is then submitted to axial compression with unloading–reloading cycles of increasing intensity. These cycles are controlled at an axial displacement rate of 5 $\mu\text{m/s}$ in loading and 1 $\mu\text{m/s}$ in unloading. During loading, this rate corresponds to a strain rate of around $3.5 \times 10^{-5}/\text{s}$ for the sample. In the pre-peak phase, the increasing intensity in axial load is controlled by the deviatoric stress value: $q = 10, 20, 40, 80, 130, 200, 300$ MPa, etc. The strain level can then be used as an indicator during the post-peak phase. At the end of each axial unloading, the deviatoric stress is held at a positive value of a few MPa in order to maintain piston contact with the sample. Triaxial tests are performed on the four samples at varying confining pressures: $p = 20, 50, 200$ and 400 MPa. As an example, Fig. 5 shows the sample stress state versus time during the triaxial test conducted at a confinement of 200 MPa.

The unconfined compression test is performed using a press without any confinement cell. For this test, the sample instrumentation is slightly different: two axial gauges and two circumferential gauges placed diametrically opposite, along with three LVDT positioned at 120°. A summary of all tests included in this campaign is provided in Table 2.

2.4 Optical observations

To complete this experimental study, optical observations were recorded in order to characterize concrete

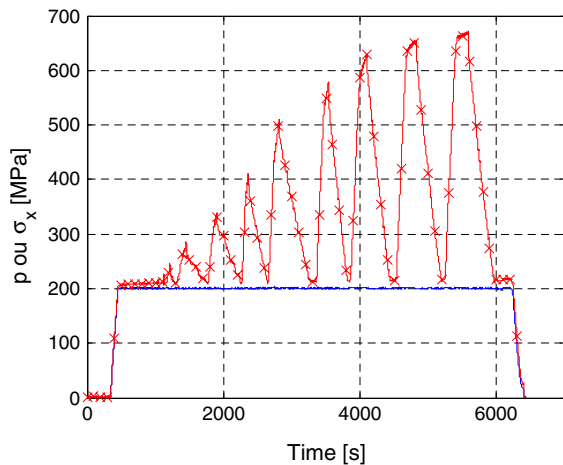


Fig. 5 Triaxial test at 200 MPa confinement (TRX200): confining pressure (-) and axial stress (×) versus time

Table 2 Summary of the cyclic tests conducted in this study

Test name	Maximum confining pressure (MPa)	q_{\max} (MPa)	Number of cycles
HYD	580	0	12
SC	0	40	16
TRX20	20	136	9
TRX50	50	210	9
TRX200	200	467	11
TRX400	400	588	10

damage in the sample. These observations took place at the mesoscopic scale (characteristic aggregate size) by use of simple binocular. All samples observed were first tested until failure, except for the one corresponding to the hydrostatic test. Table 3 summarizes the entire set of observed samples.

Meticulous preparation is required prior to undertaking an optical analysis of the post-test sample. During the initial step, the sample is immersed in epoxy resin. This step takes place in a vacuum and is

Table 3 Summary of samples submitted to optical observation

Sample name	Confining pressure (MPa)	q_{\max} (MPa)	ϵ_x max (%)
Blank	0	0	0
HYD400	400	0	2
TRX50bis	50	165	3.5
TRX650	650	850	10

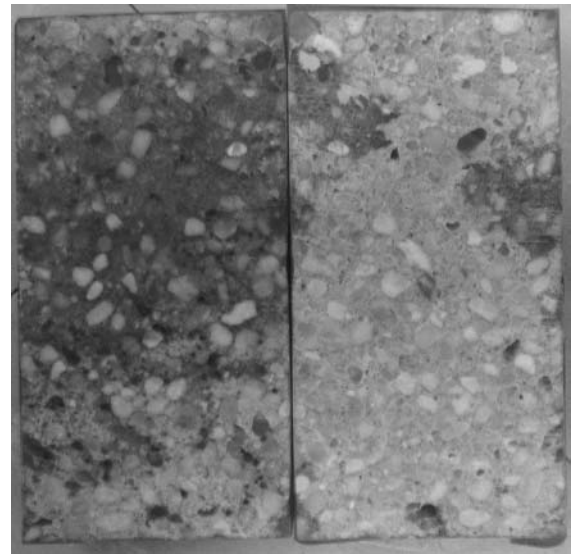


Fig. 6 HYD400 specimen prepared for optical observation: picture of half-sample after sawing (*right*), and after resin impregnation (*left*)

intended to freeze the broken sample. The sample is then diametrically cut with a diamond wire saw. Once the sample has been split into two parts, the desired sample surface is impregnated with resin. The final step consists of polishing this surface: this operation allows eliminating excess resin and improving the overall surface state. Figure 6 provides a comparison of cut faces from a sample both with and without resin impregnation. Note that if the sample is highly damaged, the initially impregnated resin spreads to the sample core.

So as to better characterize post-failure sample cracking, the observation of a pure concrete sample is taken as a reference.

3 Test results

In this section, results will be presented in the form of axial stress-strain curves. Axial strain is obtained from the axial gauge at the beginning of the test. Should the gauge fail or the measurement become meaningless, the LVDT sensor is employed for the end of the test. Circumferential strain is derived by taking the mean of the two circumferential gauge readings, whereas volumetric strain is deduced from these same two measurements in presuming that the

concrete radial strain is similar to circumferential strain, i.e.:

$$\varepsilon_v = \varepsilon_x + 2\varepsilon_\theta \quad (3)$$

3.1 Hydrostatic test

Figure 7 shows a volumetric behavior curve corresponding to a hydrostatic load with unloading–reloading cycles. The upper envelope indicates a major modification in the tangent bulk modulus of concrete. For a mean stress of less than 60 MPa, this modulus does not evolve significantly. The concrete behavior is said to be linear elastic. The first five unloading–reloading cycles are thus similar, when including the noise level. From 60 MPa on up, the tangent modulus decreases substantially, with this drop most likely being due to cement matrix damage.

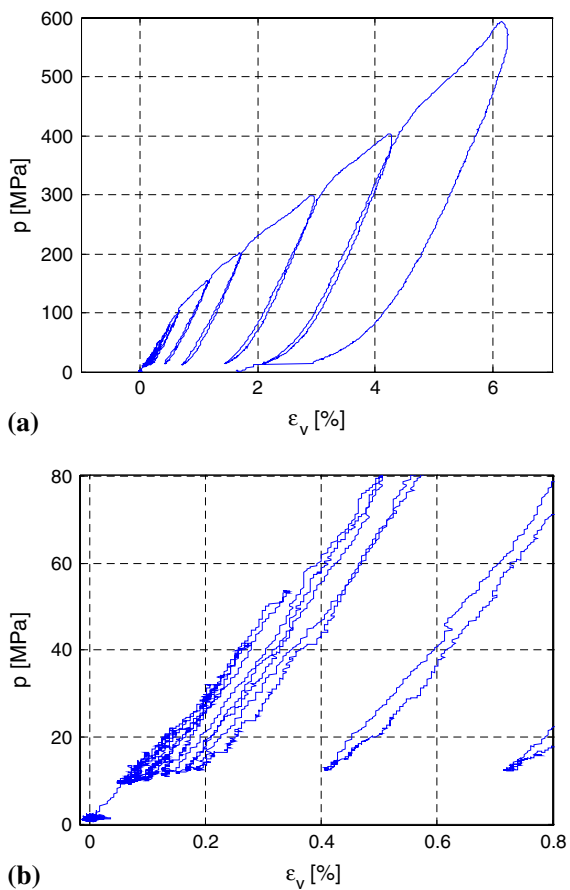


Fig. 7 Hydrostatic (HYD) test: confining pressure p versus volumetric strain ε_v : **a** full scale, **b** close-up of the first seven loading–unloading cycles

At a mean stress of about 250 MPa, an inflection point is observed, after which concrete stiffness resumes. This stiffening phase corresponds to an increase in material contact caused by the abrupt decline in porosity [21].

The unloading cycles occurring during the test allow evaluating both the irreversible strain and the evolution in residual bulk elastic modulus. The first irreversible strains begin to appear after the decrease in tangent modulus. A permanent volumetric strain of 0.02% is measured after one cycle at 80 MPa of confining pressure. For the last unloading cycle, an inelastic 4% strain is obtained for a load at 580 MPa. Note the very strong nonlinearity at the completion of unloading, which returns the residual volumetric strain of concrete to less than 2%. This sudden decrease in tangent modulus is probably due to cement matrix damage when the granular skeleton, which remains elastic, recovers its initial shape.

Figure 8 presents the bulk elastic modulus K_v corresponding to the linear part of the unloading cycle versus confining pressure. K_v values increase monotonically with pressure. This increase proves to be significant for confining pressures of below 150 MPa, at which point the cement matrix becomes heavily damaged. Afterwards, K_v increases from 14 GPa for pure concrete to 23 GPa for a 150 MPa confinement. The increase in K_v beyond 150 MPa however is very limited, since the K_v value only equals 24 GPa at 580 MPa. The volumetric behavior of concrete thus shows similarity with that of a high-friction granular material.

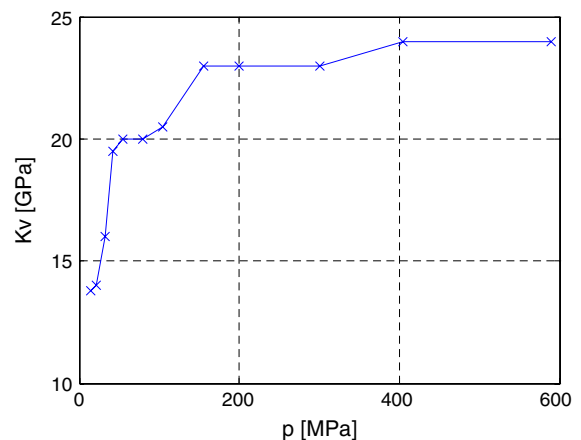


Fig. 8 Hydrostatic (HYD) test: bulk elastic modulus in unloading versus confining pressure p

Figure 9 displays a comparison of concrete optical observations between an undamaged sample and after a 400 MPa hydrostatic loading. A comparison of the two photographs shows a granular rearrangement associated with concrete compaction. This figure clearly reveals a closure of macroscopic porosity along with damage at the cement matrix/aggregate interface, also called the interfacial transition zone (ITZ) or “transition aureole”; this interface is a zone of weakness within the cement matrix [22] and can be seen on the photographs as a thin white band around the aggregates. On the sample tested along a hydrostatic loading path, the ITZ is much more distinct than on the undamaged sample, which thus reflects a localization of concrete damage on this interface that can be explained by both the weakness in this zone and the discontinuity in mechanical properties between aggregates and matrix.

Other phenomena demonstrate that the concrete has lost a sizable amount of its cohesion. When observing the surface of the sample without resin after cutting, a number of small zones are visible

where the mortar disintegrates very easily (see Fig. 10). This loss of cohesion in the cement matrix is caused by the hydrostatic load and then amplified when the sample is cut. These optical observations also reveal the presence of some unbonded or stamped aggregates. These more limited phenomena on the HYD400 sample are not at all apparent on the pure sample.

This hydrostatic test and associated optical observations provide a better understanding of the hydrostatic behavior of concrete. At low confining pressures (<150 MPa), behavior is governed by the porous and cohesive cement matrix, which when damaged leads to a strong decrease in the volumetric tangent stiffness of concrete. For intermediate confining pressures (from 150 to 400 MPa), the cement matrix loses a portion of its cohesion, in which case the concrete behaves like a compact granular stacking arrangement, i.e. elastoplastic behavior with a constant elastic unloading modulus. For the highest confining pressure level (beyond 400 MPa), the sudden drop in porosity and concrete densification

Fig. 9 Photograph of the center of the sample: reference specimens (*left*) and HYD400 test specimens (*right*)

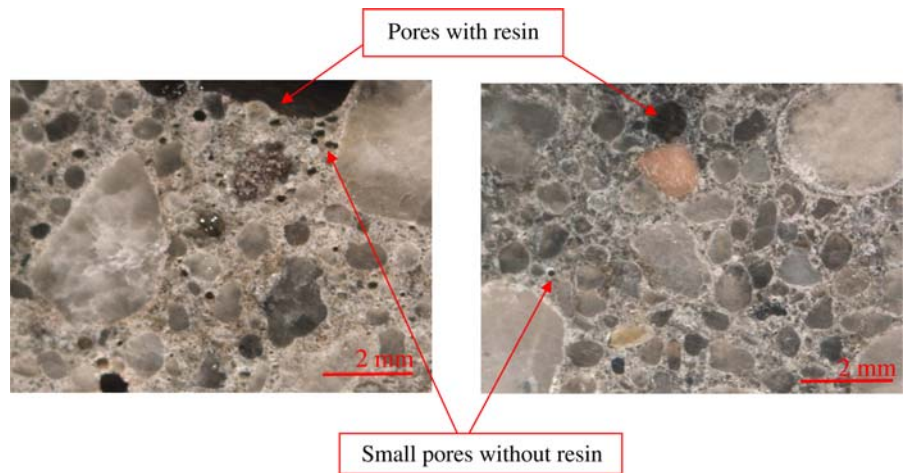


Fig. 10 Photograph of concrete at the center of the sample: reference specimens (*left*) and HYD400 specimens in a zone where the mortar is crumbling (*right*)



are both significant and constitute a rise in volumetric tangent stiffness.

The unloading behavior, which started out linear, is no longer linear at the end of unloading, with a concrete stiffness value that decreases very sharply. This phenomenon is due to the heterogeneous nature of concrete. The granular skeleton, which remains basically elastic, recovers its initial shape and causes damage to the cement matrix, which had been strongly compacted during hydrostatic compression.

3.2 Triaxial tests

It is a well-known fact that geomaterials are pressure-dependent; triaxial test results are therefore typically analyzed in the (J, σ_m) plane, where σ_m is the mean stress and J the Von-Mises stress ($J = \sqrt{3J_2}$, with J_2 being the second deviatoric stress invariant). In the present study, $J = \|q\|$, where $q = \sigma_x - p$ is the principal differential stress. An analysis of triaxial test results can then be performed by relying upon several curves:

- curves representing the principal differential stress versus axial and circumferential strains; and
- the curve representing axial stress versus volumetric strain.

For this type of test, the unloading–reloading cycles are only carried out during the axial compression phase.

3.3 Simple compression test

The simple compression test consists of a triaxial test undertaken at a zero confining pressure. Figure 11a displays a set of curves of axial stress versus strain components. For axial stress values below 20 MPa, the unloading–reloading cycles overlap, with the concrete behaving in an elastic linear manner. Young's modulus equals 33 GPa and Poisson's ratio stands at 0.16. Beyond 20 MPa of axial stress, the tangent modulus decreases continuously until reaching a peak stress at around 40 MPa. The concrete then has a softening behavior. The volumetric behavior curve (Fig. 11b) shows that the uniaxial behavior of concrete becomes dilating just after the linear elasticity phase and clearly before the peak stress.

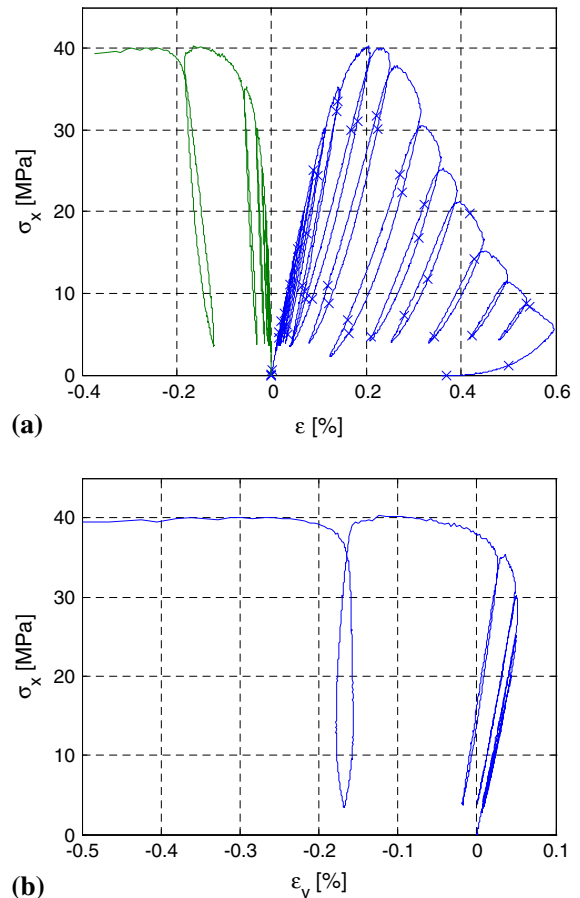


Fig. 11 Simple compression (SC) test. **a** Axial stress σ_x versus strain components ϵ_x (\times) and ϵ_θ ($-$). **b** Mean stress σ_x versus volumetric strain ϵ_v

In investigating the unloading–reloading cycles, a continuous decrease in unloading modulus is apparent during the test once the elastic phase has been completed, with a drop from 35 GPa for the first cycles to 7 GPa by the end of the test. The slight increase in stiffness, found at the beginning of compression, can be explained by the initial cracks created during drying. The subsequent decrease is caused by the gradual damage of concrete during compression. The hysteresis loops observed after the peak stress are characteristic of localized damage, which is consistent with sample observations during the test and information available from the literature [8, 23]. These findings reveal axial cracking of the sample during compression, in which case concrete behavior is characteristic of a brittle material governed by damage phenomena.

3.4 Triaxial test at 20 and 50 MPa

The triaxial test results at 20 and 50 MPa are displayed in Figs. 12 and 13. Since these two tests yield similar results, the comments offered on the curves are based primarily on the test conducted at 50 MPa of confinement, whose noise level is slightly lower.

The deviatoric part of tests depicted on the curves in Figs. 12a and 13a displays similar characteristics to those observed during the simple compression test. Following an elastic phase, the tangent modulus decreases and concrete behavior then becomes dilatant. Next, a peak stress is reached before the concrete softens.

In spite of these similarities, these figures still show the effect of confinement on concrete behavior.

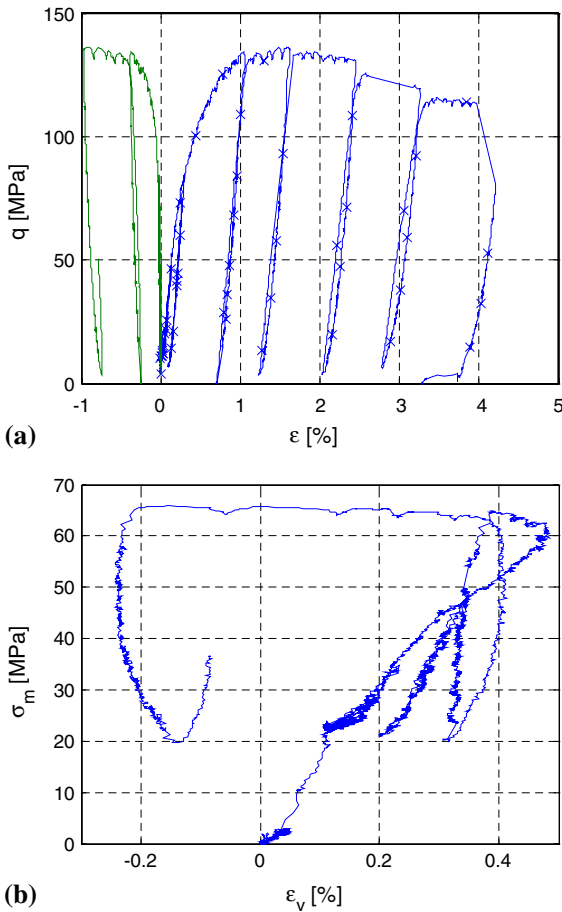


Fig. 12 Triaxial test at 20 MPa confinement (TRX20). **a** Axial stress σ_x versus deviatoric strain components ϵ_x (\times) and ϵ_θ (-). **b** Axial stress σ_x versus volumetric strain ϵ_v

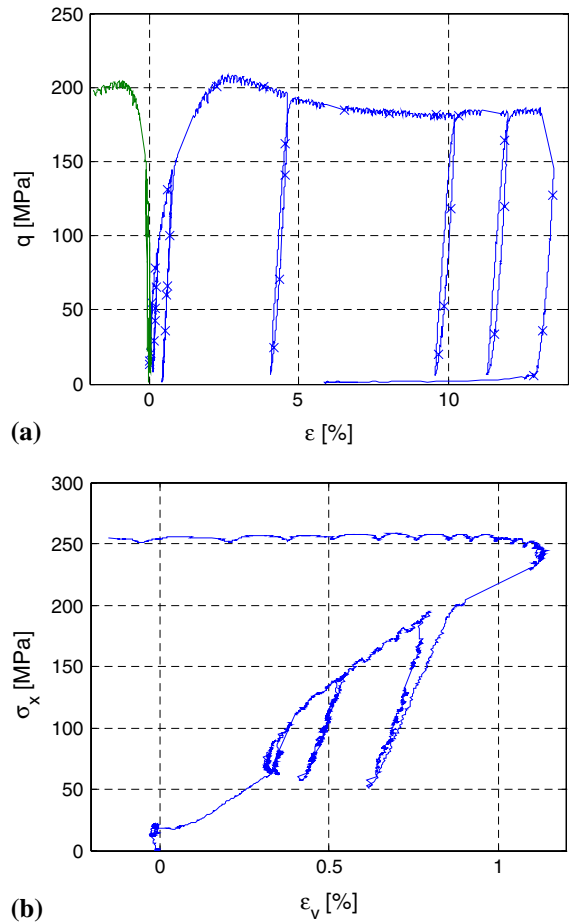
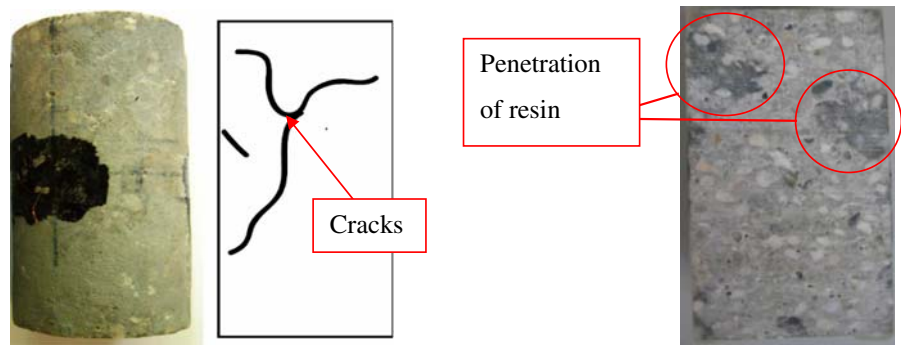


Fig. 13 Triaxial test at 50 MPa confinement (TRX50). **a** Axial stress σ_x versus deviatoric strain components ϵ_x (\times) and ϵ_θ (-). **b** Axial stress σ_x versus volumetric strain ϵ_v

A very sharp rise in strength is noticed with the maximum deviatoric stress increasing from 40 MPa for the simple compression test to 185 MPa for the TRX50 test. The contraction-to-dilatancy transition is not repeated like with the compression test just after the elastic part. As confinement increases, there is a plasticization of material before the onset of dilatancy. Moreover, the concrete becomes very ductile as the TRX50 test displays a long stress plateau, with an axial strain measured at greater than 13%.

The first unloading–reloading cycles are linear elastic. Like with the simple compression test, the material hardens slightly, followed by a modulus decrease with an increase in axial strain. This decrease, synonymous with damage, is smaller than that recorded during the simple compression test. Note that on Figs. 12 and 13, the hysteresis

Fig. 14 TRX50bis specimen after a triaxial test at 50 MPa confinement; condition of concrete on the cylinder-shaped surface (*left*) and at the center of the sample (*right*)



phenomenon observed during unloading–reloading cycles is clearly less discernible as confinement increases.

Figure 14 contains a photograph of the cylindrical face as well as a section cut of the TRX50bis sample after the triaxial test at 50 MPa confinement. The maximum axial strain thus equals 3.5%. At this strain level, the sample once again becomes perfectly consistent. Only a very thin slanting crack appears on the cylindrical face. This crack is also visible on the sample section cut (see Figs. 14 and 15), meaning the crack has spread to the sample interior without passing all the way through. On the TRX50 sample tested with cycles until reaching an axial strain of 13%, a more significant yet still quite similar damage is observed. Two slanting cracks have crossed the sample and the cement matrix is still cohesive.

An optical observation of the TRX50bis sample section cut reveals minor concrete damage. Some aggregates are unbonded and the porosity seems to have decreased slightly. On the other hand, no stripping phenomena appear on the matrix adjacent to the sawn cut. The sample essentially shows localized damage, with failure being caused by the formation of just one or two thin cracks developing inside the material.

3.5 Triaxial test at 200 and 400 MPa

Figures 16 and 17 display triaxial test results for confining pressures of 200 and 400 MPa, respectively. For a confinement of 400 MPa, the experimental device is not able to reach the peak stress; concrete behavior becomes ductile with a very high level of strain hardening. The volumetric curves beyond a certain threshold indicate however that concrete behavior changes from a contraction phase to a

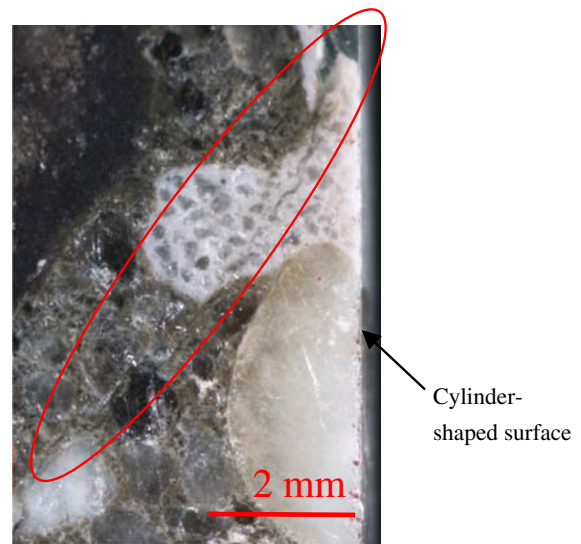


Fig. 15 Close-up of the crack on the TRX50bis specimen

dilatancy phase. This point of contraction–dilatancy transition allows defining a strain limit state for the concrete.

The unloading–reloading cycles on these tests show that Young's modulus evolves similarly as in previous tests. The variance in this modulus with respect to axial strain however is less pronounced as confining pressure increases. For the TRX400 test, Young's modulus only decreases therefore by a small amount, from 65 GPa at the beginning of axial loading to 58 GPa for an axial strain of about 6%. In addition, the hysteresis phenomenon between unloading and reloading becomes practically nonexistent for such a confinement level.

The concrete makes the transition from a very brittle behavior in the simple compression test to a ductile behavior with strain hardening subjected to a very high confinement. The study performed by Sfer

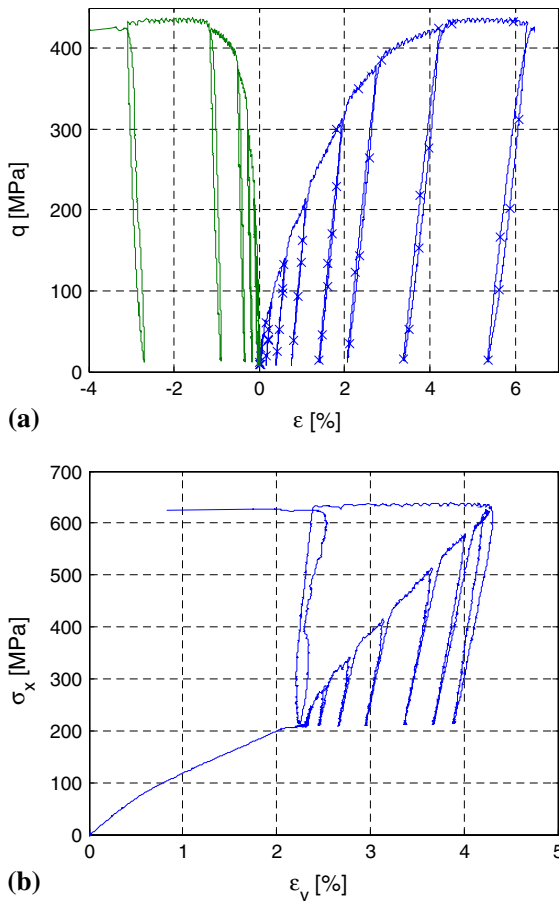


Fig. 16 Triaxial test at 200 MPa confinement (TRX200). **a** Axial stress σ_x versus deviatoric strain components ϵ_x (\times) and ϵ_θ (-). **b** Axial stress σ_x versus volumetric strain ϵ_v

indicates a similar trend but for substantially lower confining pressures [8].

In order to better understand the failure mode of concrete under high confinement, Figs. 18, 19 and 20 display the optical observations recorded on the sample after a triaxial test at a confining pressure of 650 MPa and until reaching an axial strain of 12% (see Ref. [19] for more details on this test). Figure 18 shows a photograph of the full sample section cut. A thick crack, perpendicular to the compression test axis, crosses the sample by circumventing the aggregates. Other thinner cracks featuring the same orientation are also visible on the close-up of this section cut (Figs. 19 and 20).

Figure 19 prominently shows a very high level of damage for the cement matrix of concrete. This matrix has lost its cohesion and the visible porosity

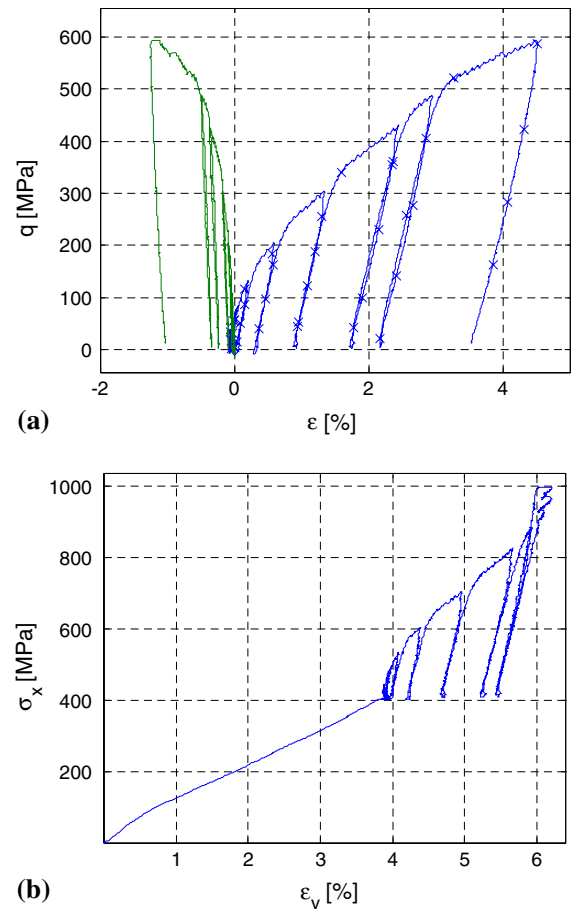


Fig. 17 Triaxial test at 400 MPa confinement (TRX400). **a** Axial stress σ_x versus deviatoric strain components ϵ_x (\times) and ϵ_θ (-). **b** Axial stress σ_x versus volumetric strain ϵ_v

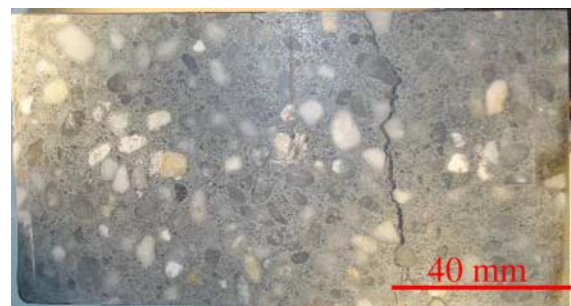


Fig. 18 The TRX650 half-sample

has completely disappeared. Around the larger aggregates, an interstice reveals the presence of considerable unbonding. Figure 20 indicates an enlarging facies of the same sample in a zone without any coarse gravel. Many small cracks are visible in

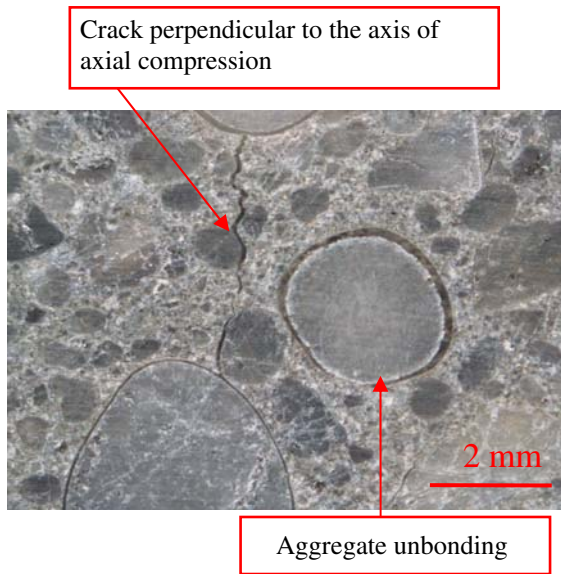


Fig. 19 Concrete damage on the TRX650 confinement specimen

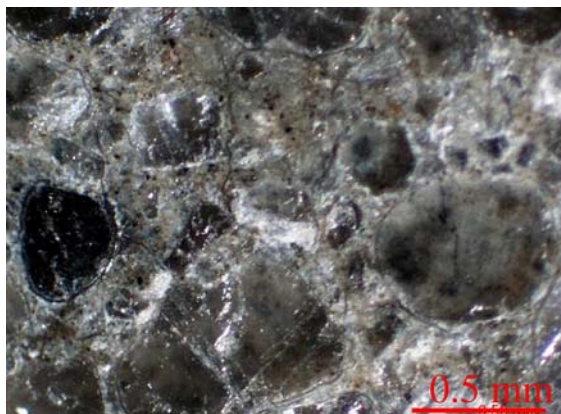


Fig. 20 Cement paste damage on the TRX650 specimen

the matrix, and this characterizes diffuse damage. The orientation of these cracks is mainly perpendicular to the axial compression direction.

4 Evolution in concrete behavior with confinement

4.1 Evolution of elastic features

The test results presented above show a major change in concrete behavior with confinement. In order to better quantify this evolution, this section of the paper

will provide a summary of the progression in concrete elastic features over the course of the previous tests. Figures 21 and 22 show, for each test, the evolution in Young’s modulus E_d and Poisson’s ratio ν_d versus axial strain ϵ_x . These parameters are identified by the average unloading–reloading cycle lines. The associated axial strain corresponds with the value obtained before initiating the unloading cycle.

Figure 21 indicates that the Young’s modulus of concrete increases monotonically with respect to confining pressure and decreases with an increase in axial strain. This figure also clearly highlights that the decrease in E_d with axial strain becomes less pronounced as confinement increases. The concrete

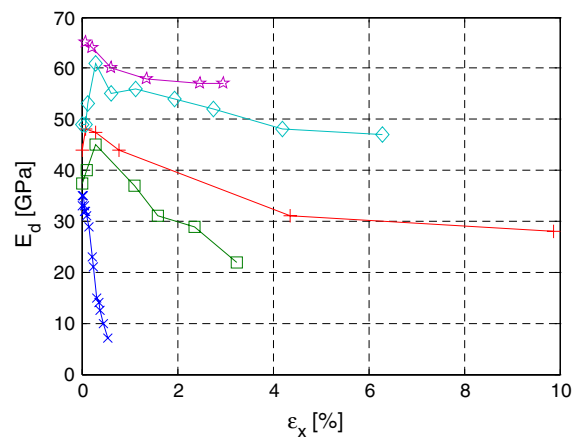


Fig. 21 Evolution in elastic stiffness with deviatoric axial strain at various pressures: (x) SC, (□) TRX20, (+) TRX50, (◇) TRX200, (☆) TRX400

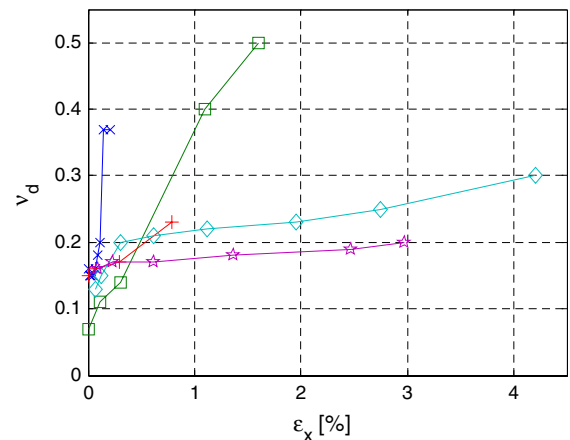


Fig. 22 Evolution in Poisson’s ratio with deviatoric axial strain at various pressures: (x) SC, (□) TRX20, (+) TRX50, (◇) TRX200, (☆) TRX400

damage, as characterized by the decrease in E_d with strain, is therefore inhibited by confinement.

The evolution in ν_d is similar with an opposite sign. Figure 22 shows that Poisson’s ratio increases considerably during the simple axial compression test. This well-known phenomenon can be explained by the opening of axial cracks during the simple compression test, which causes the dilating behavior of concrete. On the other hand, for higher confinement levels, Poisson’s ratio increases only marginally during the test, which suggests that high confinement prevents cracks from opening during the compression phase.

4.2 Strain and damage localization

For most tests, axial strain is measured simultaneously by LVDT sensors, which provides a global measurement, and an axial gauge that offers a local measurement. These two sources are complementary and allow evaluating sample strain homogeneity during testing. Figure 23a and b displays the curves of axial stress versus strains measured with the gauge and the LVDT sensor for the TRX50 and TRX200 tests. Figure 24 clearly indicates, for each test, the difference between global axial strain and local axial strain. For this figure, the measured axial strains only begin during axial compression.

For the TRX50 test, the level of strain remains very consistent until reaching the peak stress ($\epsilon_x = 3.5\%$); beyond this peak however, strain measured by the gauge is very low whereas the mean strain is very high. This loss of strain homogeneity at the peak stress level is visible for most tests at low confinement levels; it reveals strain localization, a characteristic of the type of concrete damage behavior. This localization phenomenon has also been observed by Rutland for tests at low confinement on a similar concrete [18].

On the other hand, for the TRX200 test, the strain measured by the gauge is consistent with the mean sample strain during the entire test period. This would also be true for tests at a higher confinement level. At high confinements, the strain measured on the gauge scale remains homogeneous in the sample beyond failure.

These remarks on strain localization in the sample are indeed consistent with optical observations. At low confinement, i.e. as long as confining pressure p is less than or equal to the hydrostatic elastic limit

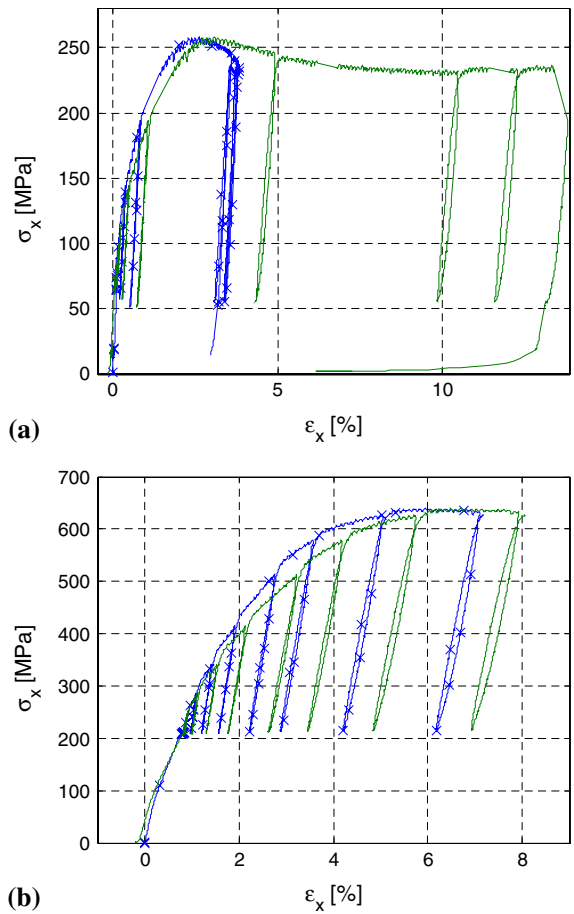


Fig. 23 Comparison of axial stress–strain curves obtained by the axial gauge (–) and the LVDT sensor (×) for two triaxial tests—TRX 50 (above) and TRX 200 (below)

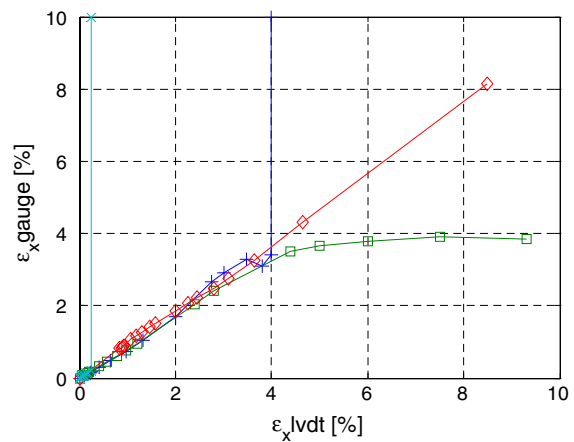


Fig. 24 Comparison of the deviatoric axial strain measured with the axial gauge and LVDT sensor for four triaxial tests: (×) SC, (+) TRX20, (□) TRX50, and (◇) TRX200

stress p_e , the cement matrix is not damaged upon completion of the hydrostatic phase, which means that concrete damage remains very localized. It is characterized by a number of cracks that cause the sample to fail. In contrast, at high confinement, the cement matrix is compacted and loses its cohesion during the hydrostatic phase. In this case, the concrete behaves like a granular stacking arrangement, which creates diffuse damage of the cement matrix during the deviatoric phase. This damage is characterized by numerous small cracks, with strain localization occurring at a scale much smaller than that of the larger aggregates.

5 Conclusion

This article has focused on the behavior of concrete under extreme loading conditions and, in particular, has sought to characterize the evolution in triaxial behavior of a standard concrete for confining pressure varying from 0 to 600 MPa. To proceed, hydrostatic and triaxial tests containing unloading–reloading cycles have been conducted on concrete samples using a high-capacity triaxial press. These tests have allowed identifying the evolution in elastic characteristics associated with unloading concrete versus both confinement and axial strain. Moreover, optical observations were performed in order to visualize the evolution in concrete damage mode at the sample center.

The cyclic hydrostatic test shows that the greatest part of cement matrix damage when submitted to hydrostatic compression occurs between 60 and 150 MPa; this test has allowed determining two confining pressures that characterize concrete behavior. Under hydrostatic loading, the concrete is linear elastic for a confining pressure of less than $p_e \sim 60$ MPa. It is of the elastoplastic type, such as a consolidated granular material, beyond a confining pressure $p_c \sim 150$ MPa.

The triaxial test results show that confinement influence on deviatoric behavior is very significant, by virtue of determining the cement matrix state before the axial compression phase. Figure 25 displays the strain limit states in the (q, σ_m) plane with their associated failure facies. These states correspond to the contraction–dilatancy transition on the triaxial volumetric curve. The entire set of limit states

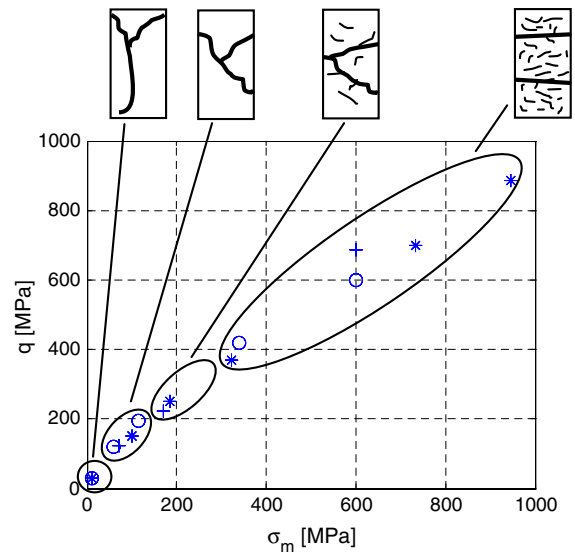


Fig. 25 Limit state points as contraction–dilatancy transitions on the volumetric behavior curves plotted in the stress space (σ_m, q) with associated failure facies: (*) limit state of Gabet's triaxial tests, (+) limit state of Gabet's proportional tests, (O) limit state of cyclic triaxial tests

proceeds from the triaxial and proportional testing performed by T. Gabet with the previously described cycle. At low confinement ($p < p_e$), the cement matrix is only slightly damaged. Failure is caused by a mechanism of considerable localized damage at the sample scale and is to be associated with a loss in strain homogeneity; this failure is characterized by a peak stress that reveals the brittle behavior of concrete. A strong decrease in axial stiffness coupled with an increase in Poisson's ratio can be observed with an increase in axial strain. A hysteresis phenomenon appears during the unloading–reloading cycles and becomes very pronounced after the peak stress. The concrete behavior is cohesive-brittle and governed by damage phenomena, in the sense of stiffness loss.

Under high confinement ($p > p_c$), the cement matrix loses a significant part of its cohesion during the hydrostatic phase. Failure under an axial load is thus caused by diffuse damage without any loss of strain homogeneity. This failure is associated with a concrete behavior that becomes dilating without reaching a peak stress. The concrete is also very ductile, with both the hysteresis phenomenon and evolution in its elastic characteristics becoming negligible during unloading cycles. Concrete behavior

tends toward that of granular material governed by plasticity, whereas the damage phenomenon observed at low confinement is inhibited.

Acknowledgments The GIGA press has been installed in the 3S-R Laboratory within the scope of a cooperative agreement signed with the French Defense Ministry's Armament Division. This research has been performed with the financial support of the Gramat Research Center (CEG, DGA). We would like to thank Dr. Eric Buzaud (CEG) for giving technical and scientific advice.

References

- Zukas JA (1992) Penetration and perforation of solids. In: Impact dynamics. Krieger Publishing Company
- Li H, Pugh D (1970) Mechanical behavior of materials under pressure. Elsevier, Amsterdam
- Kupfer HB, Gerstle KH (1973) Behavior of concrete under biaxial stresses. *J Eng Mech Div* 99(4):853–866
- Wang CZ, Guo ZH, Zhang XQ (1987) Experimental investigation of biaxial and triaxial compressive concrete strength. *ACI Mater J* 84:92–100
- Jiang LH, Huang DH, Xie NX (1991) Behavior of concrete under triaxial compressive-compressive-tensile stresses. *ACI Mater J* 88(2):181–185
- Imran I, Pantazopoulou SJ (1996) Experimental study of plain concrete under triaxial stress. *ACI Mater J* 93(6): 589–601
- Taliercio A, Berra M, Pandolfi A (1999) Effect of high-intensity sustained triaxial stresses on the mechanical properties of plain concrete. *Mag Concr Res* 51(6):437–447
- Sfer D, Ignacio C, Gettu R, Etse G (2002) Study of behavior of concrete under triaxial compression. *J Eng Mech* 128(2):156–163. doi:10.1061/(ASCE)0733-9399(2002)128:2(156)
- Bazant ZP, Bishop FC, Chang TP (1986) Confined compression tests of cement paste and concrete up to 300 Ksi. *ACI J* 33:553–560
- Burlion N, Pijaudier-Cabot G, Dahan N (2001) Experimental analysis of compaction of concrete and mortar. *Int J Numer Anal Methods Geomech* 25:1467–1486. doi: 10.1002/nag.178
- William EM, Akers SA and Reed PA (2005) Constitutive models for the triaxial behaviour of concrete. Report no. ERDC/GSL TR-05-16, Geotechnical and Structures Laboratory, US Army
- Akers SA, Phillips BR (2004) Concrete modelled as an inhomogeneous material: numerical simulations of contact detonation charges. In: 18th International symposium on the military aspects of blast and shock, Oberjettenberg
- Schmidt JM (2003) High pressure and high strain rate behaviour of cementitious materials: experiments and elastic/viscoplastic modelling. PhD thesis, University of Florida, USA
- Warren T, Fossum A, Frew D (2004) Experimental investigation of size effect in concrete fracture under multiaxial compression into low-strength (23 MPa) concrete: target characterization and simulations. *Int J Impact Eng* 30:477–503. doi:10.1016/S0734-743X(03)00092-7
- Gabet T, Malécot Y, Daudeville L (2008) Triaxial behaviour of concrete under high stresses: influence of the loading path on compaction and limit states. *Cement Concr Res* 38(3):403–412. doi:10.1016/j.cemconres.2007.09.029
- Lu X, Hsu C-TT (2007) Stress-strain relations of high strength concrete under triaxial compression. *J Mater Civ Eng* 19(3):261–268. doi:10.1061/(ASCE)0899-1561(2007)19:3(261)
- Mazars J (1986) A description of microscale and macroscale damage of concrete structures. *Eng Fract Mech* 25(5–6):729–737. doi:10.1016/0013-7944(86)90036-6
- Rutland CA, Wang ML (1997) The effects of confinement of failure orientation in cementitious materials: experimental observations. *Cement Concr Compos* 19:149–160. doi:10.1016/S0958-9465(97)00005-X
- Gabet G, Vu XH, Malecot Y, Daudeville L (2006) A new experimental technique for the analysis of concrete under high triaxial loading. In: 8th International conference on mechanical and physical behavior of materials under dynamic loading, EDP Sciences, Les Ulis. *J Phys IV* 134:635–640. doi:10.1051/jp4:2006134098
- Vu XH, Malecot Y, Daudeville L, Buzaud E (2008) Experimental analysis of concrete behavior under high confinement: effect of the saturation ratio. *Int J Solids Struct*. doi:10.1016/j.ijsolstr.2008.10.015
- Balmer GG (1949) Shearing strength of concrete under high triaxial stress: computation of Mohr's envelope as a curve. Report no. sp 23, Structural Research Laboratory, Denver
- Diamond S, Huang J (2001) The ITZ in concrete—a different view based on image analysis and SEM observations. *Cement Concr Compos* 23:179–188. doi:10.1016/S0958-9465(00)00065-2
- Torrenti JM, Benajia EH, Boulay C (1993) Influence of boundary conditions on strain softening in concrete compression test. *ASCE J Eng Mech* 119(12):2369–2384